Real-Time Observation of Instantaneous ac Stark Shift of a Vacuum Using a Zeptosecond Laser Pulse

Dandan Su(苏丹丹)[1] and Miao Jiang(江淼)[2,3*]

[1]*Key Laboratory for Laser Plasmas (Ministry of Education) and School of Physics and Astronomy, Collaborative Innovation Center for IFSA (CICIFSA), Shanghai Jiao Tong University, Shanghai 200240, China*
[2]*School of Science, China University of Mining and Technology, Beijing 100083, China*
[3]*State Key Laboratory for Geomechanics and Deep Underground Engineering, China University of Mining and Technology, Beijing 100083, China*

(Received 4 September 2023; accepted manuscript online 13 December 2023)

Based on the numerical solution of the time-dependent Dirac equation, we propose a method to observe in real time the ac Stark shift of a vacuum driven by an ultra-intense laser field. By overlapping the ultra-intense pump pulse with another zeptosecond probe pulse whose photon energy is smaller than $2mc^2$, electron–positron pair creation can be controlled by tuning the time delay between the pump and probe pulses. Since the pair creation rate depends sensitively on the instantaneous vacuum potential, one can reconstruct the ac Stark shift of the vacuum potential according to the time-delay-dependent pair creation rate.

DOI: 10.1088/0256-307X/41/1/014201

In quantum field theory,[1] the vacuum state is defined as the lowest energy eigenstate of the system. This vacuum contains all kinds of virtual particles[2] that are created and annihilated simultaneously. Changing the dynamics of the virtual particles can alter the properties of the vacuum. Usually, there are two ways to affect the virtual particles. One is to impose an additional boundary condition on the quantum vacuum, which is easier to implement, such as the Casimir effect.[3] The other may exert an external force on virtual particles. In the quantum electrodynamics (QED) realm,[4] this can be achieved by imposing an electromagnetic background field on a Dirac vacuum.

Similar to the situation of atoms in an external electric field,[5] the energy levels of a vacuum driven by intense lasers may shift. This is termed as the ac Stark shift. Since the energy levels of the vacuum state determine many other physical processes, knowing about the instantaneous energy shifts allows one to control the vacuum more accurately and to steer ultrafast QED processes in the vacuum. Thus, it is useful to observe ac Stark shift in real time. Among these processes, one of the most important is electron–positron pair (EPP) creation,[6] which is acknowledged as the most significant prediction in QED. The early studies of Heisenberg and Euler,[7] Sauter,[8] and Schwinger[9] showed that the vacuum can be broken down if the external field E is higher than the critical field $E_{\rm cr} \simeq 1.32 \times 10^{18}\,{\rm V/m}$. Many efforts have been devoted to decreasing the field strength threshold and increasing the creation yield, such as nonlinear Breit–Wheeler pair production,[10–12] the dynamical assistant Schwinger pair creation process,[13–17] and optimizing the laser pulse, etc.[18–22]

While the concept of the dynamical assistant Schwinger pair creation process[13,23] has been studied, our focus in this study lies in exploring the properties of the quantum vacuum state under a low-frequency but high-intensity laser pulse, particularly in terms of the energy and density of states. In this work, we observed that the energy levels experience periodic shifts due to the presence of the laser pulse, and the energy gap between negative and positive energies undergoes periodic compression. By introducing an additional zeptosecond pulse with a photon energy below $2mc^2$ at proper time delays, where m and c represent the electron mass and the speed of light, respectively, an EPP may or may not be created. The probability of EPP creation is closely related to the time delay between the pulses. By analyzing the probability of EPP generation with respect to the time delay, one can infer the results using the concept of ac Stark shift in the vacuum. This allows for determining the instantaneous energy gaps between the positive and negative energy. In this study, we conceived a new strategy for real-time observation of the ac Stark shift of the quantum vacuum.

In this Letter, the theoretical framework of EPP creation is first described. Then, we introduce the behavior of the vacuum energy levels in a weakly varying pulse, and present the results for the dependence of pair production yield on the time delay between the pulses and interpret the results. Finally, we give a conclusion.

Theoretical Framework. We study pair production by employing the computational quantum field theory (CQFT) approach.[24,25] In quantum field theory, all physical quantities can be expressed in terms of the field operator $\hat{\Psi}(\boldsymbol{r}, t)$. For a Dirac field, this field operator can be expanded in terms of the creation operator $\hat{d}_n^\dagger(t)$ for positrons and the annihilation operator $\hat{b}_p(t)$ for electrons, i.e.,

$$\hat{\Psi}(\boldsymbol{r}, t) = \sum_p \hat{b}_p(t)\psi_p(\boldsymbol{r}) + \sum_n \hat{d}_n^\dagger(t)\psi_n(\boldsymbol{r}). \tag{1}$$

Here, $\psi_p(\boldsymbol{r})$ and $\psi_n(\boldsymbol{r})$ are the eigenstates of the force-

*Corresponding author. Email: mjiang@cumtb.edu.cn
© 2024 Chinese Physical Society and IOP Publishing Ltd

free Dirac equation with positive and negative energies, respectively. The particle number operator for electrons is written as

$$\hat{N}(t) = \hat{\Psi}_+^\dagger(\boldsymbol{r},\, t)\hat{\Psi}_+(\boldsymbol{r},\, t), \tag{2}$$

where the positive frequency part of the field operator is $\hat{\Psi}_+(\boldsymbol{r},\, t) = \sum_p \hat{b}_p(t)\psi_p(\boldsymbol{r})$. To obtain the time-dependent particle yield, we calculate the expectation value $N(t) = \langle\langle \text{vac}||\hat{N}(t)||\text{vac}\rangle\rangle$, where $||\text{vac}\rangle\rangle$ is the vacuum state. The time-dependent field operators $\hat{\Psi}(\boldsymbol{r},\, t)$ fulfill the following Heisenberg equations of motion:

$$i\hbar\frac{\partial\hat{\Psi}(\boldsymbol{r},\, t)}{\partial t} = [\hat{\Psi}(\boldsymbol{r},\, t), \hat{H}], \tag{3}$$

with the quantum field Hamilton operator $\hat{H}$,

$$\hat{H} = \int \hat{\Psi}^\dagger(\boldsymbol{r},\, t)\hat{H}_{\text{D}}\hat{\Psi}^\dagger(\boldsymbol{r},\, t)d^3\boldsymbol{r} \tag{4}$$

with $\hat{H}_{\text{D}}$ representing the first quantized single-particle Dirac Hamiltonian. Substituting Eq. (4) into Eq. (3) yields the time-dependent Dirac equation

$$i\hbar\frac{\partial\hat{\Psi}(\boldsymbol{r},\, t)}{\partial t} = \hat{H}_{\text{D}}\hat{\Psi}(\boldsymbol{r},\, t). \tag{5}$$

Here $\hat{H}_{\text{D}}$ is expressed as

$$\hat{H}_{\text{D}} = c\boldsymbol{\alpha}\cdot\Big[\boldsymbol{p} - \frac{e\boldsymbol{A}(\boldsymbol{r},\, t)}{c}\Big] + \beta mc^2 + eV(\boldsymbol{r},\, t), \tag{6}$$

where $\boldsymbol{\alpha}$ and β are Dirac matrices.

Alternatively, the field operator $\hat{\Psi}(\boldsymbol{r},\, t)$ can also be expanded as

$$\hat{\Psi}(\boldsymbol{r},\, t) = \sum_p \hat{b}_p\psi_p(\boldsymbol{r},\, t) + \sum_n \hat{d}_n^\dagger\psi_n(\boldsymbol{r},\, t). \tag{7}$$

Comparing Eq. (1) with Eq. (7), the time-dependent and time-independent creation and annihilation operators can be equated through the Bogoliubov transforms:

$$\hat{b}_p(t) = \sum_p G(^+|_+)\hat{b}_p(t) + \sum_n G(^+|_-)\hat{d}_n^\dagger, \tag{8a}$$

$$\hat{d}_n^\dagger(t) = \sum_p G(^-|_+)\hat{b}_p(t) + \sum_n G(^-|_-)\hat{d}_n^\dagger. \tag{8b}$$

Here, $G(^+|_+) = \int d\boldsymbol{r}\langle\psi_p(\boldsymbol{r})|\psi_p(\boldsymbol{r},\, t)\rangle$, $G(^+|_-) = \int d\boldsymbol{r}\langle\psi_p(\boldsymbol{r})|\psi_n(\boldsymbol{r},\, t)\rangle$, $G(^-|_+) = \int d\boldsymbol{r}\langle\psi_n(\boldsymbol{r})|\psi_p(\boldsymbol{r},\, t)\rangle$, and $G(^-|_-) = \int d\boldsymbol{r}\langle\psi_n(\boldsymbol{r})|\psi_n(\boldsymbol{r},\, t)\rangle$ denote the projection of the solution of the time-dependent Dirac equation $\psi_{p,\,n}(\boldsymbol{r},\, t)$ onto the force-free eigenstate $\psi_{p,\,n}(\boldsymbol{r})$. So far, the created electrons per unit volume $\frac{1}{V}$ can be further derived as

$$\begin{aligned} N(t) &= \sum_n\sum_p\int d\boldsymbol{r}\frac{1}{V}\langle\langle\text{vac}||\hat{\Psi}_+^\dagger(\boldsymbol{r},\, t)\hat{\Psi}_+(\boldsymbol{r},\, t)||\text{vac}\rangle\rangle \\ &= \sum_n\sum_p\frac{1}{V}\langle\langle\text{vac}||\hat{d}_n^\dagger(t)\hat{d}_n(t)||\text{vac}\rangle\rangle \\ &= \sum_n\sum_p\frac{1}{V}|G(^-|_+)|^2, \end{aligned} \tag{9}$$

and the momentum distribution is

$$\rho(p,\, t) = \sum_p\frac{1}{V}|G(^-|_+)|^2. \tag{10}$$

In Eqs. (9) and (10), the space- and time-dependent numerical solutions $\psi_p(\boldsymbol{r},\, t)$ of the Dirac equation are crucial, and can be obtained by propagating the time-dependent Dirac equation with the split-operator technique [26] under periodic boundary conditions.

In our calculations, the two laser pulses are expressed by $\boldsymbol{A}_1(t) = (0,\, 0,\, A_{1,\,z}(t))$ and $\boldsymbol{A}_2(t) = (0,\, 0,\, A_{2,\,z}(t))$ with an explicit form of

$$\begin{aligned} A_{1,z}(t) &= A_{10}\text{exp}\Big(-\frac{t^2}{2\tau_1^2}\Big)\cos(\omega_1\, t), \\ A_{2,z}(t) &= A_{20}\text{exp}\Big[-\frac{(t-\delta t)^2}{2\tau_2^2}\Big]\cos(\omega_2\, t). \end{aligned} \tag{11}$$

Here, A_{10} and A_{20} are the laser amplitudes and δt is the time delay between two pulses; τ_1 and τ_2 define the duration of the two laser pulses. The two laser frequencies satisfy $\omega_1 \ll \omega_2$. We have employed the dipole approximation in this study, and we present our simulation results in the following.

Energy Shift and State Redistribution. We first show the energy spectra of the vacuum dressed by the intense laser pulse $\boldsymbol{A}_1(t)$. This dressing of the vacuum can be considered as exciting the negative energy states to higher energy states, resulting in modification of the gap and redistribution of the energy eigenstates in the negative continua. [6,27] Since the electric field of the driving laser field periodically changes, the eigenstate energies will be periodically shifted, similar to the well-known ac Stark shift observed in atomic physics.

It is well known that the so-called "hole" theory is a phenomenological picture of quantum vacuum states. The theory is used to explain the positive and negative energy solutions of the Dirac equation. [28] The negative energy eigenstates of the Dirac equation are deemed as positrons by charge conjugation and the positive ones can be regarded as electrons. The gap between the positive and negative energy states of the force-free Dirac equation is $2mc^2$, while this shrinks if the vacuum is dressed by the intense laser pulse. The one-dimensional and three-dimensional calculations are different, but this does not alter the fact that the shrinkage of the vacuum state's energy gap is solely determined by $V(\boldsymbol{r},\, t)$, where $V(\boldsymbol{r},\, t)$ represents the vector potential. Regardless of the dimensional case, a higher value of $V(\boldsymbol{r},\, t)$ leads to a greater gap shrinkage. Consequently, our discussion focuses solely on the energy change of the vacuum state in the one-dimensional scenario. The simplified one-dimensional Hamiltonian is

$$\hat{H}_{\text{D}} = c\sigma_1\cdot\Big(p_z - \frac{e\boldsymbol{A}_1(t)}{c}\Big) + \sigma_3 mc^2. \tag{12}$$

Due to the electric field $\boldsymbol{E}_1(t) = -\frac{1}{c}\frac{\partial\boldsymbol{A}_1(t)}{\partial t}$, $\boldsymbol{E}_1(t) = (0,\, 0,\, E_{1,\,z}(t))$, the instantaneous eigenstates of Eq. (12) for $t = t_0$ cannot reflect the influence of the electric field $\boldsymbol{E}_1(t = t_0)$ since $\boldsymbol{E}_1(t = t_0)$ should be obtained by knowing $\boldsymbol{A}_1(t_0 + dt)$ and $\boldsymbol{A}_1(t_0 - dt)$ numerically. Thus, to get the correct instantaneous eigenstates shifted by the electric field, we need to change from the A-gauge with $(\phi,\, A)$ to the V-gauge $(\phi',\, A')$. [29] The A-gauge and V-gauge can

be related by a function $\chi(x)$ and satisfy the following transformation formulae:

$$\phi' = \phi - \frac{\partial\chi(x)}{\partial t}, \tag{13a}$$

$$A' = A + \nabla\chi(x). \tag{13b}$$

Now, considering the A-gauge as ($\phi = 0$, $A = \boldsymbol{A}_1(t)$), we aim to find ϕ' in the V-gauge when $A' = 0$. To determine ϕ', we can proceed with the following derivations. First, by substituting $A' = 0$ and $A = \boldsymbol{A}_1(t)$ into Eq. (13b), we obtain the expression for $\chi(x)$. Then, employing $\phi = 0$ and $\chi(x)$ in Eq. (13a), we derive the value of ϕ'. In our case, ϕ' is $eE_{1,z}(t)z$.

After the gauge transformation, the Hamiltonian can be rewritten as

$$\hat{H}_{\rm D} = c\sigma_1 \cdot p_z + \sigma_3 mc^2 + eE_{1,z}(t)z. \tag{14}$$

Since the creation process of EPPs primarily occurs on the spatial scale of the Compton wavelength $\lambda_{\rm e}$, we propose calculating the eigenstates of Eq. (14) within a spatial range of z from 0 to $\lambda_{\rm e}$. As depicted in Fig. 1, at a given moment, as z increases linearly from 0 to $\lambda_{\rm e}$, the energy levels of the vacuum exhibit a shift, causing a reduction in the energy gap. The reduction is $E_{1,z}(t)\lambda_{\rm e}$, so the energy gap becomes $G = 2mc^2 - E_{1,z}(t)\lambda_{\rm e}$.

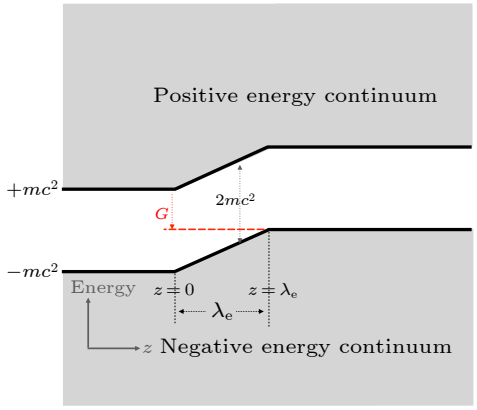

Fig. 1. Sketch of gap shrinkage: $G = 2mc^2 - E_{1,z}(t)\lambda_{\rm e}$ is the energy gap when the vacuum is dressed.

We quantitatively illustrate the gap reduction over time in Fig. 2. These eigenstates are obtained through numerical diagonalization of a $2n \times 2n$ Hamiltonian matrix. The positive and negative states are discretized in both momentum and spatial coordinates by n. The results obtained by this $2n \times 2n$ Hamiltonian matrix are consistent with those acquired through numerical diagonalization of a 2×2 Hamiltonian matrix, as determined by Eq. (14) for different momenta $p_z = n\frac{2\pi}{L}$ of positive and negative states. For these calculations, we employ periodic boundary conditions, where box length $L = 1$ and $n = 1024$. Since gap change is related to $2mc^2 - E_{1,z}(t)\lambda_{\rm e}$, in order to ensure $E_1(t)\lambda_{\rm e} = E_{1,z}(t)L$, the electric field should be redefined as $E = E_{1,z}(t)\lambda_{\rm e}$ when we calculate the eigenstates in Fig. 2.

In Fig. 2(a), we plot the instantaneous eigenstate energies dressed by $\boldsymbol{A}_1(t)$. The energies are shifted by the laser field, and the state density is redistributed. One can see that the energy gap between positive and negative energy states fluctuates with the period t_{p1}, therein $t_{p1} = \frac{2\pi}{\omega_1}$. This is consistent with the phenomenon that occurs in atomic physics since the energy shift is proportional to the instantaneous intensity. In order to conveniently describe the dynamics, in Fig. 2(a) four points are marked by A, B, C, and D, indicating different eigenstate energies at different instantaneous intensities of the laser pulse. When the instantaneous laser intensity is maximal, the energy gap is minimal.

In Fig. 2(b), we present $\rho_E = 1/\Delta E$, which can be considered as the eigenstate density. Here, ΔE is the energy interval of eigenstates. Compared with the green curves (corresponding point C), where there is no shift and the curves start from $\pm mc^2$, the starting points for the red curves (corresponding points A and D) move to $\pm 0.88mc^2$, and for the blue curves (corresponding point B) they move to $\pm 0.93mc^2$. Thus, the energy gap is $2mc^2$ for the green, $1.76mc^2$ for the red, and $1.86mc^2$ for the blue curves. The energy gap can also be calculated using the formula $2mc^2 - E_{1,z}(t)\lambda_{\rm e}$, which is approximately equal to $2mc^2$, $1.85mc^2$, and $1.76mc^2$, and these values agree with the energy gap shown by the green, blue, and red curves, respectively.

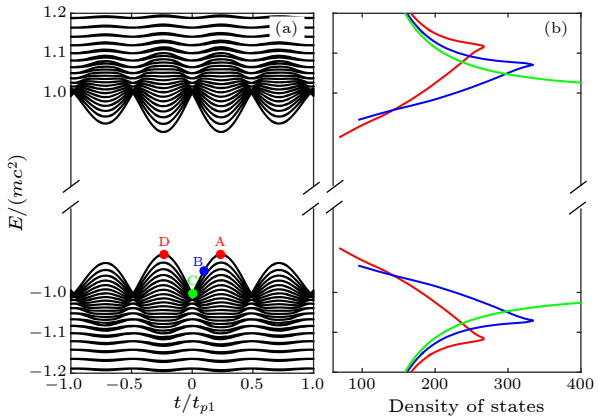

Fig. 2. (a) The energies of the instantaneous energy eigenstates in the strong electric field. The marked A and D correspond to the vacuum state with the largest instantaneous electric field. For C, it is zero. The horizontal and vertical axes represent time and energy, respectively; $t_{p1} = \frac{2\pi}{\omega_1}$ is the laser period. (b) The densities of the instantaneous eigenstates for different times corresponding to the marked A, B, and C in (a). The other parameters are $A_{10} = 5.0mc^2$, $\omega_1 = 0.05mc^2$, and $\tau_1 = t_{p1}$.

In addition, the intense laser pulse $\boldsymbol{A}_1(t)$ leads to a redistribution of the eigenstates of the vacuum. Different from the green curves, whose maximum eigenstate densities are located at $\pm 1.02mc^2$, the locations of the peaks for eigenstate density move to $\pm 1.07mc^2$ and $\pm 1.13mc^2$ for blue and red curves, respectively, as presented in Fig. 2(b). Thus, the optimal photon energy for the EPP creation process will be shifted accordingly. Although the laser pulse $\boldsymbol{A}_1(t)$ cannot trigger the EPP creation process alone because of its low frequency and insufficient intensity, it can still affect the creation process by dressing the vacuum and triggering the ac Stark shift.

EPP Creation in a Dressed Vacuum. We investigate

the creation of EPPs in a vacuum dressed by an intense laser $A_1(t)$. This creation process enables us to observe the ac Stark shift of the vacuum in real time. Since the EPP creation process can be viewed as the coupling of negative energy states to positive ones, different energy structures can lead to different creation processes.

In Fig. 3(a), the red curve is the total creation yield as a function of ω_2 with a time delay of $\delta t \simeq 0.25t_{p1}$. For comparison, EPP creation by $\boldsymbol{A}_2(t)$ alone is presented by the black-dotted curve. By increasing ω_2 gradually, the EPP probability changes accordingly. The EPP yields significantly increase when ω_2 approaches $2mc^2$. The reason for this is that the system can already conquer the energy gap. This results in EPP creation by absorbing one ω_2. This is within expectations. However, the two curves show noteworthy differences when $\omega_2 < 1.85mc^2$. That is due to the fact that absorbing one ω_2 will induce the probability of pair creation only if the vacuum is dressed by $\boldsymbol{A}_1(t)$. In Fig. 3(b), we show the ratio of the total yield from the vacuum with and without the dressing field $\boldsymbol{A}_1(t)$. The decreased energy gap of the dressed vacuum leads to a significant enhancement of EPP creation, which can be regarded as the dynamical assistant Schwinger pair creation process.

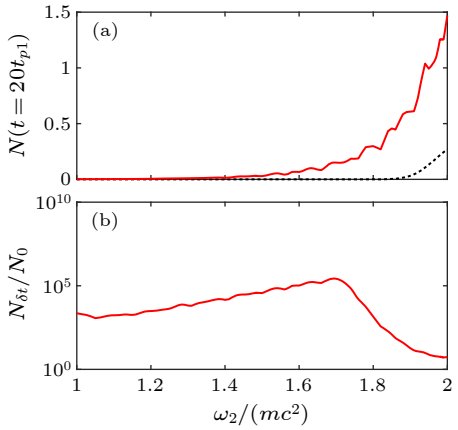

Fig. 3. (a) The EPP yield as a function of the frequency ω_2. The red curve is a result of the combination of $\boldsymbol{A}_1(t)$ and $\boldsymbol{A}_2(t)$ with a time delay $\delta t \simeq 0.25t_{p1}$, $t_{p1} = \frac{2\pi}{\omega_1}$. The parameters for laser pulse $\boldsymbol{A}_1(t)$ are $A_{10} = 5.0mc^2$, $\omega_1 = 0.05mc^2$, and $\tau_1 = t_{p1}$. For laser pulse $\boldsymbol{A}_2(t)$, they are $A_{20} = 0.01mc^2$ and $\tau_2 = \tau_1$. For comparison, the result of $A_1(t) = 0$ is plotted with the black-dotted curve, where there is no dressing of the vacuum. (b) The ratio of the total yield, which is $N_{\delta t\simeq 0.25t_{p1}}/N_0$. $N_{\delta t\simeq 0.25t_{p1}}$ and N_0 are the red and black-dotted curves in (a), respectively. The spatial size is $z = 1.0$.

Real-Time Observation of the ac Stark Shift. Based on the above analysis, we propose a strategy to observe the ac Stark shift of the vacuum driven in real time by the strong laser field $\boldsymbol{A}_1(t)$. We overlap $\boldsymbol{A}_1(t)$ with another ultrashort laser pulse with $\omega_2 < 2mc^2$ and a pulse duration much smaller than t_{p1}. Due to the ac Stark shift driven by $\boldsymbol{A}_1(t)$, ω_2 can overcome the squeezed gap and create EPPs. On the other hand, if the ultrashort laser pulse $\boldsymbol{A}_2(t)$ emerges when the temporary $\boldsymbol{A}_1(t)$ is maximal, the energy gap is not squeezed and ω_2 is insufficient to excite negative energy states. Hence, the EPP creation probability depends on the time delay between the two pulses.

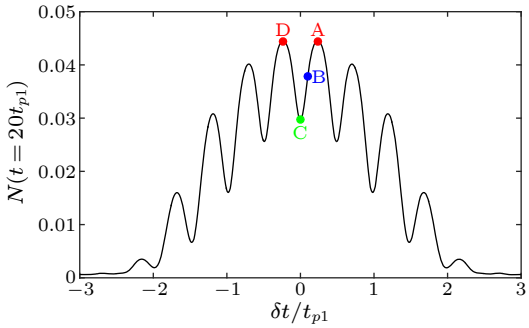

Fig. 4. Total yield $N(t = 20t_{p1})$ of the created EPPs as a function of the time delay δt between two laser pulses. The parameters of the laser pulse $\boldsymbol{A}_1(t)$ are $A_{10} = 5.0mc^2$, $\omega_1 = 0.05mc^2$, and $\tau_1 = t_{p1}$. The parameters of the laser pulse $\boldsymbol{A}_2(t)$ are $A_{20} = 0.01mc^2$, $\omega_2 = 1.8mc^2$, and $\tau_2 = 0.1t_{p1}$. The time delay of the marked A, B, C, and D are $\delta t \simeq 0.25t_{p1}$, $\delta t \simeq 0.1t_{p1}$, $\delta t = 0$, and $\delta t \simeq -0.25t_{p1}$, respectively. The spatial size is $z = 1.0$.

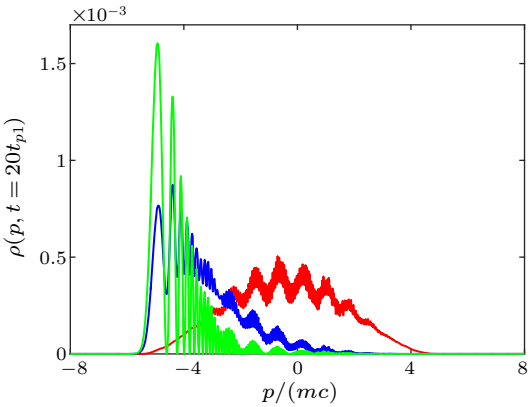

Fig. 5. The momentum spectra of the created positrons. The time delays of the red, blue, and green lines are $\delta t \simeq 0.25t_{p1}$, $\delta t \simeq 0.10t_{p1}$, and $\delta t = 0$, respectively. Here, $t_{p1} = \frac{2\pi}{\omega_1}$. The parameters for laser pulse $\boldsymbol{A}_1(t)$ are $A_{10} = 5.0mc^2$, $\omega_1 = 0.05mc^2$, and $\tau_1 = t_{p1}$. For laser pulse $\boldsymbol{A}_2(t)$, they are $A_{20} = 0.01mc^2$, $\omega_2 = 1.80mc^2$, and $\tau_2 = 0.1\tau_1$.

As the time delay δt changes from $\delta t = -3t_{p1}$ to $\delta t = 3t_{p1}$, the total yields fluctuate with the frequency $2\omega_1$, as shown in Fig. 4. The four points marked by A, B, C, and D coincide with the points in Fig. 2(a). The fluctuation of the EPP probability can be understood in another way. For example, when the time delay is $\delta t \simeq 0.25t_{p1}$, $\boldsymbol{A}_2(t)$ emerges approximately at the point of $\boldsymbol{A}_1(t) \simeq 0$, where the temporary $\boldsymbol{E}_1(t)$ is maximal. Once the electron in the "Dirac sea" absorbs one ω_2 and jumps to virtual states just below mc^2, with the temporary maximum $\boldsymbol{E}_1(t)$, it is able to free these virtual states via tunneling. Since the tunneling ionization rate exponentially depends on the laser electric field, the EPP probability is very sensitive to δt. When the zeptosecond pulse appears at C in Fig. 4, where $\boldsymbol{E}_1(t) = 0$, the EPP probability is expected to be zero. However, due to the nonzero pulse duration of the zeptosecond laser pulse, $\boldsymbol{A}_2(t)$ may overlap with parts

of the nonzero part of $\boldsymbol{E}_1(t)$, leading to the noticeable EPP probability at C.

We also show the momentum spectra of the created positrons in Fig. 5 for the three corresponding time delays marked by A, B, and C in Fig. 4. When the delay is $\delta t \simeq 0.25t_{p1}$, the EPPs are mostly created by the tunneling ionization of $\boldsymbol{A}_1(t)$, as discussed above. In this case, the momentum mainly distributes around 0, as is expected. For other time delays, such as $\delta t \simeq 0.1t_{p1}$ and $\delta t = 0$, the positron momentum is shifted by $\boldsymbol{A}_1(t')$, where t' is the moment at which the zeptosecond pulse emerges.

This is similar to the ionization process of electrons in a combination of long-pulse near-infrared and short-pulse extreme ultraviolet light fields. The ionized electron satisfies Newton's equation $m\frac{dv}{dt} = eE_{\rm IR}(t)$, where $E_{\rm IR}(t) = -\frac{1}{c}\frac{\partial A_{\rm IR}(t)}{\partial t}$ is the near infrared light field. Consequently, Newton's equation becomes $m\frac{dv}{dt} = -\frac{e}{c}\frac{\partial A_{\rm IR}(t)}{\partial t}$. According to this equation, the momentum $mv(t)$ of the ionized electron should satisfy equation $mv(t)+eA_{\rm IR}(t)/c = P$, where P is constant. Hence, compared with P, the momentum $mv(t)$ of the ionized electron is shifted by $A_{\rm IR}(t)/c$. Now, let us discuss the EPP creation process. For a time delay of approximately $\delta t \simeq 0.25t_{p1}$, the value of $\boldsymbol{A}_1(t')$ is approximately zero. This leads to a symmetric momentum distribution, as depicted by the red curve in Fig. 5. Alternatively, for a time delay of approximately $\delta t \simeq 0t_{p1}$, the value of $\boldsymbol{A}_1(t')$ is approximately $-5.0mc$, resulting in a right shift in the momentum distribution. This shift is represented by the green curve in Fig. 5. The dynamic process of the created particles contributes to the asymmetry observed in the blue and green curves. All curves contain two oscillatory behaviors. The presence of slow oscillations can be understood as resonances within a one-dimensional quantum-mechanical scattering problem. On the other hand, the faster oscillations can be attributed to the non-monochromatic nature of the laser pulse $\boldsymbol{A}_2(t)$.[30,31]

Conclusion and Outlook. In a manner similar to birefringence and polarization of the quantum vacuum, the ac Stark effect of the quantum vacuum takes place when an external field attains a significant intensity. Notably, the probabilities associated with these effects are nonlinearly dependent on the amplitude of the field. Thus, this strong field should be treated as a classical electromagnetic field. In order to detect these quantum effects on short time scales in real time, a process on shorter time scales, such as electron–positron pair creation, is a perfect choice. With this strong field, the spatial effect of the field also affects the properties of the quantum vacuum state. It is an intriguing problem for future research whether a focusing laser could affect the properties of the quantum vacuum state.

In this study, we propose a strategy for observing in real time the ac Stark shift of a vacuum induced by an ultra-intense laser pulse. Upon the irradiation of an intense laser pulse, the energy levels of the vacuum are periodically shifted, and the energy gap between positive and negative energy states is periodically squeezed. By introducing a zeptosecond laser pulse, whose photon energy is smaller than $2mc^2$, the combined pulses with a proper time delay can significantly enhance the EPP creation probability. Since the EPP creation probability sensitively depends on the instantaneous energy gap, one may retrieve the ac Stark shift of the vacuum according to the delay-dependent EPP probability.

Acknowledgements. D. D. Su thanks Professor F. He and Dr. Y. S. Cao for the helpful discussion. This work was supported by the National Natural Science Foundation of China (Grant Nos. 12304341 and 11974419), the National Key R&D Program of China (Grant Nos. 2021YFA1601700 and 2018YFA0404802), and the Strategic Priority Research Program of Chinese Academy of Sciences (Grant No. XDA25051000). Simulations were performed on the π supercomputer at Shanghai Jiao Tong University.

References

[1] Peskin M 2018 *An Introduction To Quantum Field Theory* (New York: CRC Press)
[2] Hoi I C, Kockum A F, Tornberg L, Pourkabirian A, Johansson G, Delsing P, and Wilson C 2015 *Nat. Phys.* **11** 1045
[3] Casimir H B G 1948 *Indag. Math.* **10** 261
[4] Greiner W and Reinhardt J 2009 *Quantum Electrodynamics* (Berlin: Springer)
[5] He F, Ruiz C, Becker A, Thumm U, and Atomic J O P B 2011 *Mol. Opt. Phys.* **44** 211001
[6] Fillion-Gourdeau F M C, Lorin E, and Bandrauk A D 2013 *Phys. Rev. Lett.* **110** 013002
[7] Heisenberg W and Euler H 1936 *Z. Phys.* **98** 714
[8] Sauter F 1931 *Z. Phys.* **69** 742
[9] Schwinger J 1951 *Phys. Rev.* **82** 664
[10] di Piazza A 2016 *Phys. Rev. Lett.* **117** 213201
[11] Golub A, Villalba-Chávez S, and Müller C 2022 *Phys. Rev. D* **105** 116016
[12] Zhao J, Hu Y T, Lu Y *et al.* 2022 *Commun. Phys.* **5** 15
[13] Schützhold R, Gies H, and Dunne G 2008 *Phys. Rev. Lett.* **101** 130404
[14] Jiang M, Su D D, Lin N S and Li Y J 2021 *Chin. Phys. B* **30** 070306
[15] Jiang M, Su W, Lv Z Q, Lu X, Li Y J, Grobe R, and Su Q 2012 *Phys. Rev. A* **85** 033408
[16] Kohlfürst C, Queisser F, and Schützhold R 2021 *Phys. Rev. Res.* **3** 033153
[17] Ren Y L, Luo C Q, and Sitiwaldi I 2023 *Phys. Rev. A* **107** 012210
[18] Sang H B, Jiang M, and Xie B S 2013 *Chin. Phys. Lett.* **30** 111201
[19] Li Z L, Sang H B, and Xie B S 2013 *Chin. Phys. Lett.* **30** 071201
[20] Olugh O, Li Z, and Xie B 2020 *Phys. Lett. B* **802** 135259
[21] Li L J, Mohamedsedik M, and Xie B S 2021 *Phys. Rev. D* **104** 036015
[22] Kohlfürst C, Ahmadiniaz N, Oertel J, and Schützhold R 2022 *Phys. Rev. Lett.* **129** 241801
[23] Hebenstreit F and Fillion-Gourdeau F 2014 *Phys. Lett. B* **739** 189
[24] Braun J W, Su Q, and Grobe R 1999 *Phys. Rev. A* **59** 604
[25] Cheng T, Su Q, and Grobe R 2010 *Contemp. Phys.* **51** 315
[26] Bauke H and Keitel C H 2011 *Comput. Phys. Commun.* **182** 2454
[27] Fillion-Gourdeau F, Lorin E, and Bandrauk A D 2012 *J. Phys. A* **45** 215304
[28] Dirac P A M 1930 *Proc. R. Soc. Lond. A* **126** 360
[29] Su W, Jiang M, Lv Z Q, Li Y J, Sheng Z M, Grobe R, and Su Q 2012 *Phys. Rev. A* **86** 013422
[30] Hebenstreit F, Alkofer R, Dunne G V, and Gies H 2009 *Phys. Rev. Lett.* **102** 150404
[31] Aleksandrov I A, Plunien G, and Shabaev V M 2017 *Phys. Rev. D* **96** 076006